Springer

KSME

Journal of Mechanical Science and Technology 30 (9) (2016) 4325~4335
www.springerlink.com/content/1738-494x(Print)/1976-3824(Online)
DOI 10.1007/s12206-016-0847-5

Design optimization of 3PRS parallel manipulator using global performance indices †

S. Ramana Babu[1,*], V. Ramachandra Raju[2] and K. Ramji[3]

[1]*Department of Mechanical Engineering, Raghu Engineering College, Visakhapatnam, 531121, India*
[2]*Department of Mechanical Engineering, Jawaharlal Nehru Technological University, Kakinada, 532111, India*
[3]*Department of Mechanical Engineering, Andhra University, Visakhapatnam, 53003, India*

(Manuscript Received January 5, 2015; Revised December 28, 2015; Accepted May 16, 2016)

Abstract

This paper presents an optimal kinetostatic design method for a general 3PRS (Prismatic-revolute-spherical) spatial parallel manipulator by formulating a multi-objective optimization problem considering the performance indices are as the objective functions. Three performance criteria--Global conditioning index (GCI), Global stiffness index (GSI) and workspace volume-were formulated and the effect of actuator layout angle on the performance indices was studied. A multi-objective evolutionary algorithm based on the Control elitist non-dominated sorting genetic algorithm (CENSGA) was adopted to find the final approximation set. The optimal geometric parameters that yield minimal compliance with larger workspace volume and improved dexterity are suggested for a general 3PRS parallel manipulator. For the optimal design, it is shown that global isotropy and global stiffness of the platform is improved at the cost of workspace reduction.

Keywords: CENSGA; GA; GCI; GSI; Pareto front; Workspace volume

1. Introduction

Parallel kinematic machines with fewer DOF (Degrees of freedom) have attained the focus of researchers due to their advantages in terms of simple structure, reduction in manufacturing cost and easy to control when compared with higher DOF PKMs (Parallel kinematic machines). The 6-DOF Stewart platform was designed for use as an aircraft simulator by Stewart [1]. Even though the 6-DOF parallel manipulators have as many inherent advantages of parallel manipulators in terms of high stiffness, high accuracy and high load carrying capacity, but which are not always required for many applications in practice. As an outstanding representation of the limited-DOF parallel manipulators with coupling of translation and rotation, the 3PRS (Prismatic-revolute-spherical) manipulator has been applied to many aspects because of compact architecture and excellent kinematic performance. Some applications of the 3PRS parallel manipulators are the famous Sprint Z3 head made by the DS Technologies Company [2, 3] in Germany and also as a telescope application proposed originally by Carretero et al. [4], friction stir welding by Han et al. [5] and so on. Some theoretical research results of this manipulator have been published in past years; the kinematics and workspace analysis of the 3PRS manipulator is investigated by Tsai et al. [6] and Zhang et al. [7]. Although these mechanisms have different methods in actuator arrangement, they can be considered as the same type of mechanism because it can be solved using the same kinematics technique. Li and Xu [8] presented a kinematic analysis for a general type of 3PRS parallel manipulator with adjustable actuator layout angle. Chen et al. [9] provided a comparison study in terms of motion transmissibility between sprint Z3 and A3 tool head, which is based on 3RPS parallel manipulator.

The performance of a parallel manipulator is highly dependent on the architectural parameters of the mechanical structure; these parameters must be selected appropriately in order to achieve better workspace characteristics. The optimal design problem of parallel manipulators consists of finding a set of design parameters of the architecture for attaining an optimal performance criterion; it becomes an inevitable step for designing and developing of parallel manipulators. Optimal design procedures for parallel manipulators are focused on only one main characteristic, such as dexterity [10], kinematic isotropy [11] and workspace [12], velocity/force transmission index [13] and also stiffness [14, 15], to characterize its performance. Lu et al. [16] introduced a comprehensive dexterity criterion that integrates the condition number and manipulability simultaneously. However, considering only a single objective may not yield an acceptable design. A parallel manipulator designed for total workspace volume will result in a manipulator with undesirable kinematic characteristics,

*Corresponding author. Tel.: +91 8922248001, Fax.: +91 8922248011
E-mail address: ramanababu76@gmail.com
† Recommended by Associate Editor Kyoungchul Kong

such as poor dexterity and more compliance, so real world engineering design problems are characterized by many conflicting objectives. Lara-Molina et al. [17] performed the optimal design of a spatial Stewart-Gough platform based on multi-objective optimization by considering the global condition index, Global play load index (GPI) and Global gradient index (GGI) are as the objectives and it is solved by Multi-objective evolutionary algorithm (MOEA). Kelaiaia et al. [18] presented an approach for dimensional synthesis of parallel manipulators in order to maximize the performance (workspace, stiffness, kinematic, dynamic performance) using the Strength Pareto evolutionary algorithm-II (SPEA-II). Wu [19], Ganesh et al. [20], Guohua et al. [21] introduced two indices, one for translation and other for rotation for the stiffness characterization and optimization along the workspace volume.

The 3PRS parallel manipulator has recently been prototyped as machining center, but the effective design method of this manipulator for optimal performance is not extensively studied in the literature. The design optimization methodology for 3PRS parallel manipulator was proposed and solved by Carretero et al. [22] in order to maximize the dexterous workspace volume; they also suggested the optimal architectural parameters. Li and Xu [23] formulated an optimization problem for the general 3PRS parallel manipulator with the goal of reaching a compromise between two performance indices GDI (Global dexterity index) and Space utility ratio (SUR); it is solved as a single objective problem by assigning different weights to the objectives in a weighted sum objective function. Liu et al. [24] presented the optimization methodology for 3PRS manipulator by considering the error index as the objective function. Pond et al. [25] performed the architectural optimization of a three 3PRS variants for parallel machining by considering the dexterity and workspace volume are as the objectives, and also compared the performance of these manipulators. Zhang [26] presented an interval based optimization of 3PRS parallel manipulator to optimize the design parameters for maximum workspace.

In all the design methodologies presented so far for a 3PRS manipulator, the stiffness is not considered in the design process. Stiffness is an important factor to evaluate the performance of parallel manipulators because high stiffness can lead to high precision and high speed of machining. The low stiffness of links/joints may lead to large compliant displacements when an external wrench is applied at the end-effecter. The compliant displacements in parallel kinematic machines produce negative effects on static, fatigue strength, accuracy and dynamic stability (vibration). Therefore, stiffness analysis became a primary importance in design of limited DOF parallel kinematic machines in order to select the appropriate size, shape and material of the geometrical components and actuators.

Moreover, the optimal design of parallel kinematic machine by considering multiple criteria is formulated as a single objective optimization problem in the weighted sum approach, which provides only one solution for a design problem at a time for the assigned weights to the component objectives. This is actually a fatal one for practical design purposes because it is difficult to predict any application in advance and to know whether a particular design is the only possible solution. However, a multi-objective optimization with several criteria provides a Pareto optimal solution set; the designer can choose an appropriate solution to the particular application.

In the present work the kinetostatic design methodology for a general 3PRS parallel manipulator with adjustable actuator layout angle is presented. The stiffness performance index, called global stiffness index (GCI) [27], giving direct insight into the influence of design parameters on the stiffness, is adopted along with the two other performance indices, GCI and workspace volume. To ensure the isotropy of the stiffness and well conditioned workspace with considerable size, the optimal parameters have to be investigated. The stiffness index is formulated by using the stiffness matrix of the given mechanism, since the global stiffness matrix is derived as a compliance model by considering the actuator compliance, leg axial and bending compliances. Three performance indices--GCI, GSI and workspace volume--are investigated and optimal solutions are found by solving a multi-objective optimization problem using controlled elitist non-dominated sorting genetic algorithm (CENSGA) proposed by Deb and Goel [28]. This algorithm maintains a proper balance between the exploitation and exploration for maintaining diversity among the solutions of the individual non-dominated fronts.

The organization of the paper is as follows. Sec. 2 briefly gives a geometric description of the general 3PRS parallel manipulator. The kinematic analysis and Jacobian matrix derivation are described in Secs. 3 and 4, respectively. In Sec. 5 workspace analysis is presented; in Sec. 6 stiffness analysis is carried-out. Performance indices and their significance are explained in Sec. 7. After that a multi-objective optimization is described in Sec. 8, and the results are discussed in Sec. 9. Finally the paper concludes in Sec. 10.

2. Geometric description of manipulator

The CAD model for a 3PRS mechanism, shown in Fig. 1, is composed of a moving platform, a fixed base and three supporting limbs with identical kinematic structure. Each limb connects the fixed base to the moving platform by a 'P' joint, 'R' joint and 'S' joint in a sequence, where the 'P' joint is actuated by linear actuator; thus the moving platform is attached to the base by three identical PRS linkages. The geometry of the mechanism is shown in Fig. 2 in which a fixed Cartesian reference coordinate frame $O\{x,y,z\}$ is attached at the center point 'O' of the fixed base platform $\Delta A_1A_2A_3$ and a moving coordinate frame $P\{u,v,w\}$ is attached on the moving platform at point P which is the center point of the triangle $\Delta B_1B_2B_3$. The vertices of the fixed triangle A_1, A_2, A_3 that lie on the circle of radius 'a', the three links C_iB_i of length l intersects the $u-v$ plane at points B_1, B_2, B_3 which lie on a circle of radius 'b'. The sliders of the 'P' joints are re-

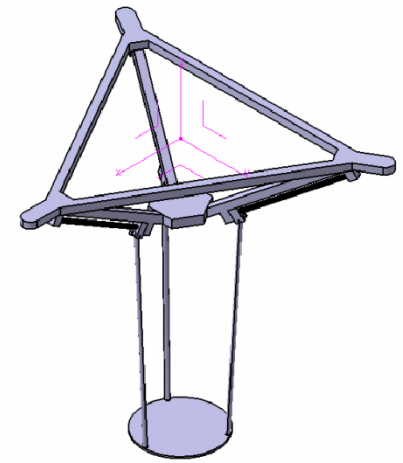

Fig. 1. CAD model of 3PRS manipulator.

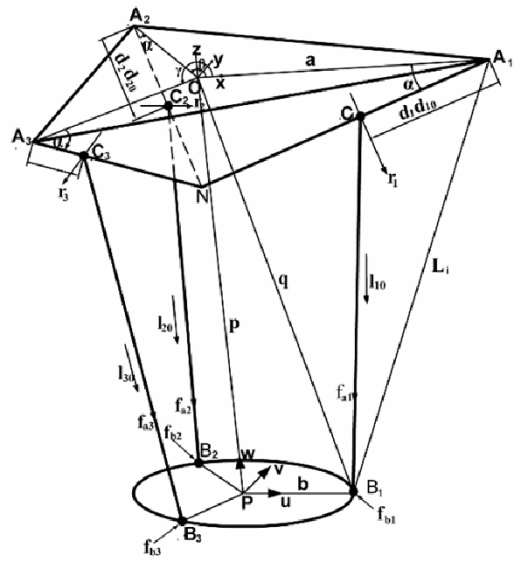

Fig. 2. 3PRS spatial parallel manipulator.

stricted to move along the rails between A_i and N. The angle α is measured from the fixed base to rail A_iN which is defined as the actuator layout angle. Angle β is defined from the x-axis to OA_2 in the fixed frame and also from the u-axis to PB_2 in the moving frame. Similarly, the angle γ is measured from the x-axis to OA_3 in the fixed frame and u-axis to PB_3 in the moving frame. In the following discussions we assign that $\beta = 120^0$ and $\gamma = 120^0$.

3. Kinematic modeling

Let $\mathbf{d} = [\mathrm{d}_1\ \mathrm{d}_2\ \mathrm{d}_3]^{\mathrm{T}}$ be the vector of the three joint variables and $\mathbf{X} = [p_x\ p_y\ p_z\ \psi\ \theta\ \varphi\ ]$ be the vector of Cartesian variables which describe the position and orientation of the moving platform, where φ, ψ, θ are Euler angles rotating about the ZXY axes of the fixed reference frame. In the inverse position kinematics the actuated joint variables for a given position and orientation of the end-effecter is solved. Let $\mathbf{I}_{i0}$ be the unit vector along C_iB_i, d_i be the linear displacement of the i_{th} actuator; $\mathbf{d}_{i0}$ is the corresponding unit vector along A_iN, $\mathbf{q}_i$ is the position vector pointing from O to i_{th} spherical joint and $\mathbf{r}_i$ is the unit vector of the revolute joint. In addition, let $\mathbf{a}_i = \overline{OA_i}$ and $b_i = \overline{PB_i}$ be the position vectors of the vertices in fixed and moving platforms, respectively; referring to Fig. 1 the vector-loop equation for the i_{th} limb can be written as

$$\mathbf{L}_i = d_i\mathbf{d}_{i0} + l\mathbf{I}_{i0}, \tag{1}$$

$$\mathbf{L}_i = \mathbf{q}_i - \mathbf{a}_i, \tag{2}$$

where $\mathbf{L}_i$ is the vector pointing from A_i to B_i and the position of spherical joint $\mathbf{q}_i = \mathbf{p} + \boldsymbol{b}_i$, $\mathbf{p} = \begin{bmatrix} p_x & p_y & p_z \end{bmatrix}^T$. Solving Eq. (2) leads to the inverse kinematic solution of a prismatic joint as

$$d_i = (\mathbf{L}_i \cdot \mathbf{d}_{i0}) + \sqrt{(\mathbf{L}_i \cdot \mathbf{d}_{i0})^2 - \mathbf{L}_i \cdot \mathbf{L}_i + l^2}. \tag{3}$$

There exist two solutions for each actuator; thus, there are eight possible solutions for a given position and orientation. Here only negative square root is selected to yield a solution where the three legs are inclined inward from top to bottom.

4. Jacobian matrix

The vector loop for the i_{th} link can be written as

$$\mathbf{p} + \mathbf{b}_i = \mathbf{a}_i + d_i\mathbf{d}_{i0} + l\mathbf{I}_{i0}. \tag{4}$$

Differentiating both sides of Eq. (4) with respect to time yields

$$\mathbf{v}_p + \boldsymbol{\omega}_p \times \mathbf{b}_i = \dot{d}_i + l\boldsymbol{\omega}_i \times \mathbf{I}_{i0} \tag{5}$$

where $\mathbf{v}_p$ and $\boldsymbol{\omega}_p$ are the linear and angular velocities of the moving platform, respectively; $\dot{d}_i$ is the velocity of the i_{th} linear actuator and $\boldsymbol{\omega}_i$ is the angular velocity of the link C_iB_i. The passive variable $\boldsymbol{\omega}_i$ can be eliminated by dot multiplying both sides of Eq. (5) with $\mathbf{I}_{i0}$ which gives

$$\mathbf{I}_{i0} \cdot \mathbf{v}_p + (\mathbf{b}_i \times \mathbf{I}_{i0}) \cdot \boldsymbol{\omega}_p = \dot{d}_i\, \mathbf{I}_{i0} \cdot \mathbf{d}_{i0}. \tag{6}$$

The above equation can be written in a matrix form as

$$\mathbf{J}_x \dot{\mathbf{X}} = \mathbf{J}_q \dot{\mathbf{d}}, \tag{7}$$

where

$$\mathbf{J}_x = \begin{bmatrix} (\mathbf{I}_{10})^T & (\mathbf{b}_1 \times \mathbf{I}_{10})^T \\ (\mathbf{I}_{20})^T & (\mathbf{b}_2 \times \mathbf{I}_{20})^T \\ (\mathbf{I}_{30})^T & (\mathbf{b}_3 \times \mathbf{I}_{30})^T \end{bmatrix}, \tag{8}$$

$$\mathbf{J}_q = \begin{bmatrix} \mathbf{I}_{10} \cdot \mathbf{d}_{10} & 0 & 0 \\ 0 & \mathbf{I}_{20} \cdot \mathbf{d}_{20} & 0 \\ 0 & 0 & \mathbf{I}_{30} \cdot \mathbf{d}_{30} \end{bmatrix}. \tag{9}$$

Let $\dot{\mathbf{X}} = \begin{bmatrix} \mathbf{v}_p & \boldsymbol{\omega}_p \end{bmatrix}^T$, $\dot{\mathbf{d}} = \begin{bmatrix} d_1 & d_2 & d_3 \end{bmatrix}^T$ be the vectors of the moving platform velocities and the actuated joint rates, respectively. Eq. (7) can be expressed as

$$\dot{\mathbf{d}} = \mathbf{J}\dot{\mathbf{X}}, \tag{10}$$

where $\mathbf{J} = \mathbf{J}_q^{-1}\mathbf{J}_x$ is a 3×6 matrix; Eq. (10) yields the inverse velocity solutions of the 3PRS parallel manipulator.

5. Workspace analysis

The workspace of a parallel manipulator is one of the most important criteria, which reflects its working capacity. So it is necessary to analyze the shape and size of the workspace for enhanced applications of parallel manipulators. While designing a practical manipulator, the physical constraints of the kinematic chains, such as limits of the linear actuators, leg interferences and limitations on the passive joints are to be considered. The prismatic stroke constraint imposed on each leg is $d_{\min} \le d_i \le d_{\max}$, where d_i is the displacement of the i_{th} joint given by Eq. (3); $d_{\min}$ and $d_{\max}$ are the minimum and maximum strokes of the actuator, respectively. The limits on the cone angle of a spherical joint are to be considered because of the difficulties in manufacturing of spherical joints; the cone angle is the angle between the links and axis of symmetry of each socket. The leg interference is also to be considered in the evaluation of the minimum distance between two cylinders in order to avoid collision. The discrete numerical search algorithm is adopted to find the shape and size of the workspace volume; the volume is quantified by the expression

$$V = \sum_{Z_i=Z_{\min}}^{Z_{\max}} \sum_{\theta_z=0}^{2\pi} \left(\frac{1}{2}\rho_i^2 \Delta\theta_z \Delta z\right), \tag{11}$$

where ρ_i is polar ray, $\Delta\theta_z$ angle of increment in rotation about Z axis and Δz is a small increment along Z axis.

6. Stiffness analysis of 3PRS manipulator

The stiffness matrix of a PKM that relates the external wrench consists of forces and moments exerted on the moving platform to its deformation by the following relation as

$$\mathbf{W} = \mathbf{K}\delta\mathbf{X}, \tag{12}$$

where $\mathbf{W}$ is the wrench vector acting on the moving platform, $\Delta\mathbf{X}$ is the deformation vector of moving platform, $\mathbf{K}$ is the generalized stiffness matrix. This externally applied wrench imposed on the end-effecter is to be equilibrated by the wrenches of actuation/constraint forces in the joint space. This can be represented mathematically as

$$\mathbf{W} = \mathbf{J}^T\mathbf{f}, \tag{13}$$

where $\mathbf{J}$ is the Jacobian matrix that relates the infinitesimal motion between the sub serial chains and moving platform, and $\mathbf{f}$ is a force vector in the sub serial chains of the manipulator. The joint rate coordinates are transformed to the end-effecter coordinates by the following relation:

$$\delta\mathbf{q} = \mathbf{J}\delta\mathbf{X}, \tag{14}$$

where $\delta\mathbf{q}$ is the vector representing the infinitesimal motion of sub serial chains; by assuming each individual element of PKM is linearly elastic, Hook's law is given as

$$\mathbf{f} = \bar{\mathbf{K}}\delta\mathbf{q}, \tag{15}$$

$$\mathbf{W} = \mathbf{K}\delta\mathbf{X}, \tag{16}$$

where

$$\mathbf{K} = \mathbf{J}^T\bar{\mathbf{K}}\mathbf{J}. \tag{17}$$

Eq. (16) can be expressed in terms of compliance as

$$\delta\mathbf{X} = \mathbf{C}\mathbf{W}, \tag{18}$$

where $\mathbf{C}$ is a generalized compliance matrix and it can be expressed as

$$\mathbf{C} = \mathbf{K}^{-1}. \tag{19}$$

The generalized compliance matrix represents how much a moving platform would deform under the applied wrench $\mathbf{W}$; the three compliances causing the end-effecter to deformation are actuator flexibility, leg bending and axial deformations. The above equation is considered for the three compliances as

$$\delta\mathbf{X}_n = \mathbf{C}_f\mathbf{W}, \delta\mathbf{X}_b = \mathbf{C}_b\mathbf{W}, \delta\mathbf{X}_a = \mathbf{C}_a\mathbf{W}, \tag{20}$$

where subscripts n, b, a indicate the deformation along the sliders due to the force on the nut, bending and axial deformation of the legs. respectively. The total deformation is given as

$$\delta\mathbf{X} = \delta\mathbf{X}_n + \delta\mathbf{X}_b + \delta\mathbf{X}_a = \mathbf{C}_G\mathbf{W}, \tag{21}$$

where the total generalized compliance matrix $\mathbf{C}_G$ is given as

$$\mathbf{C}_G = \mathbf{C}_n + \mathbf{C}_b + \mathbf{C}_a = \mathbf{K}_n^{-1} + \mathbf{K}_b^{-1} + \mathbf{K}_a^{-1}, \tag{22}$$

where

$$\mathbf{K}_n = \mathbf{J}_n^T\bar{\mathbf{K}}_n\mathbf{J}_n, \mathbf{K}_b = \mathbf{J}_b^T\bar{\mathbf{K}}_b\mathbf{J}_b, \mathbf{K}_a = \mathbf{J}_a^T\bar{\mathbf{K}}_a\mathbf{J}_a. \tag{23}$$

The total generalized stiffness matrix considering the three types of compliances can be written as

$$\mathbf{K}_G = \mathbf{C}_G^{-1}. \tag{24}$$

The three Jacobian matrices transforming the three types of compliances into the end-effecter compliance can be found by the principle of duality between statics and kinematics, which can be expressed as

$$\mathbf{J}_n = \mathbf{B}^{-1}\mathbf{A}, \mathbf{J}_b = \begin{bmatrix} (\mathbf{r}_1)^T & (\mathbf{b}_1 \times \mathbf{r}_1)^T \\ (\mathbf{r}_2)^T & (\mathbf{b}_2 \times \mathbf{r}_2)^T \\ (\mathbf{r}_3)^T & (\mathbf{b}_3 \times \mathbf{r}_3)^T \end{bmatrix} \text{ and } \mathbf{J}_a = \mathbf{A}, \tag{25}$$

where

$$\mathbf{A} = \begin{bmatrix} (\mathbf{I}_{10})^T & (\mathbf{b}_1 \times \mathbf{I}_{10})^T \\ (\mathbf{I}_{20})^T & (\mathbf{b}_2 \times \mathbf{I}_{20})^T \\ (\mathbf{I}_{30})^T & (\mathbf{b}_3 \times \mathbf{I}_{30})^T \end{bmatrix}, \tag{26}$$

$$\mathbf{B} = \begin{bmatrix} (\mathbf{d}_{10})^T \mathbf{I}_{10} & 0 & 0 \\ 0 & (\mathbf{d}_{20})^T \mathbf{I}_{20} & 0 \\ 0 & 0 & (\mathbf{d}_{30})^T \mathbf{I}_{30} \end{bmatrix}. \tag{27}$$

The local stiffness matrices $\bar{\mathbf{K}}_n$, $\bar{\mathbf{K}}_b$, $\bar{\mathbf{K}}_a$ can be expressed as

$$\bar{\mathbf{K}}_n = diag(k_{ni}), \bar{\mathbf{K}}_b = diag(k_{bi}), \bar{\mathbf{K}}_a = diag(k_{ai}), \tag{28}$$

where

k_{ni} linear stiffness coefficient of the nut along the slider
k_{bi} bending stiffness coefficient
k_{ai} axial stiffness coefficient of the leg.

7. Performance measures

7.1 Global condition Index

Dexterity is an important issue for design, trajectory planning and control of manipulators. The dexterity of a manipulator can be the ability of the manipulator to arbitrarily change its position and orientation; dexterity is measured in terms of the Jacobian matrix. The condition number of a Jacobian matrix is expressed as

$$k = \|\mathbf{J}\| \|\mathbf{J}^{-1}\|, \tag{29}$$

where $\mathbf{J}$ is called as Jacobian matrix is given by Eq. (10); the condition number signifies the error amplification factor between the joint rate errors to task space errors. The condition number depends on the manipulator configuration. The condition number varies from one at isotropic configurations to infinity at singular configurations, so this is also defined as the measure of the degree of ill-conditioning of the Jacobian matrix. The reciprocal of the condition number ($1/k$) is referred to as the conditioning index, which is the local measure of performance of the manipulator at a particular pose of the end-effecter within the workspace. To evaluate the global behavior of a manipulator over the workspace, the GCI is expressed as

$$\text{GCI} = \frac{\int_w (\frac{1}{k}) dw}{\int_w dw}, \tag{30}$$

where w is the workspace and k is a condition number.

7.2 Global stiffness Index

If an external wrench exerts on the moving platform, there is a deformation along different directions which can be regarded as being distributed on an ellipsoid sphere, with the lengths of major axis and minor axis being the maximum and minimum value of the deflections respectively. This deformation is dependent on the manipulator's stiffness and also on the external wrench. The manipulator stiffness affects the position accuracy of the device, so stiffness is considered as an important performance index. The GSI is the inverse of the condition number of the stiffness matrix integrated over the reachable workspace by the volume of the workspace, which can be expressed mathematically as

$$\text{GSI} = \frac{\int_w (\frac{1}{k_c}) dw}{\int_w dw}, \tag{31}$$

where $k_c = \|\mathbf{K}_G\| \|\mathbf{K}_G^{-1}\|$, the global stiffness matrix $\mathbf{K}_G$ is described in Eq. (24).

8. Multi-objective optimization

A multi-objective-optimization problem has a number of objective functions usually conflicting with each other that are to be minimized or maximized; a general form of the multi-objective minimization problem is expressed as

$$\min \mathbf{F}(\mathbf{X}) = \min \ [f_1(\mathbf{X}), f_2(\mathbf{X}), \ldots\ldots f_n(\mathbf{X})], \tag{32}$$

Subjected to

$$\mathbf{G}(\mathbf{X}) \le 0, \tag{33}$$

$$\mathbf{H}(\mathbf{X}) = 0 \tag{34}$$

where $\mathbf{X}$ is the vector of design variables; $\mathbf{F}(\mathbf{X})$ is the vector of objective functions that represents the optimality criteria, $\mathbf{G}(\mathbf{X})$ is the vector of constraint functions that describe the limiting functions, $\mathbf{H}(\mathbf{X})$ is the vector of constraint functions that describes the design prescriptions. The desired solution is in the form of trade off or compromise among the solutions that would optimize all objectives simultaneously; the optimal

trade off solutions among the objectives is called as Pareto optimal solutions and a curve formed by joining all these solutions is known as Pareto optimal front. The performance evaluations regarding with positioning and orientation capabilities, velocity responses, static behavior can be identified for the manipulator design. The positioning and orientation capability is represented by the size of the workspace volume, whereas the velocity responses can be represented by the GCI obtained by evaluating the Jacobian matrix. The static behavior can be evaluated by computing the stiffness components by reducing the global stiffness matrix; it is characterized by GSI. The multi-objective function $\mathbf{F}(\mathbf{X})$ is formulated with GCI, GSI and workspace volume as its component functions. The problem of achieving optimal results from the formulated multi-objective optimization problem depends upon selection of a proper optimization technique.

8.1 Controlled elitist non-dominated sorting genetic algorithm

It is well known that elitist Multi-objective evolutionary algorithms (MOEA) have better convergence characteristics than the non-elitist MOEAs, a number of elitist MOEAs, such as strength Pareto evolutionary algorithm SPEA [29], Pareto-archived evolution strategy PAES [30], etc. Later Deb et al. [31] suggested NSGA-II a fast elitist MOEA, from the simulation results on a number of difficult test problems. They reveal that NSGA-II outperforms the PAES and SPEA in converging to a true Pareto-optimal set with diversified solutions. Thereafter, they argue that NSGA-II can have uncontrolled elitism in certain problems; they introduced CENSGA to control the extent of elitism and also they implemented on five complex test problems. In all simulation results CENSGA yields a better convergence than the original NSGA-II. So the preferred multi-objective evolutionary algorithm to solve this optimization problem is the CENSGA, a variant of NSGA-II for controlling the extent of the elite members of the population and to maintain the diversity of the population for convergence to a final approximation set. The concept of CENSGA is almost the same as that of NSGA-II, but there is a difference in the elite preserving mechanism and in selection strategy.

In CENSGA all non-dominated fronts participate in the selection process through geometric distribution; at least one chromosome from each non-dominated front will be represented in the new population; whereas in NSGA-II the solutions from high ranked fronts only will take part in the creation of a new population. So the population obtained in CENSGA will be more diverse than that obtained in NSGA-II. In CENSGA a combined population $\mathbf{R}_t = \mathbf{P}_t \cup \mathbf{Q}_t$ of size 2N is formed, and then R_t is sorted according to non-domination. Since all previous and current population members are included in $\mathbf{R}_t$, elitism is ensured. The maximum number of individuals allowed in the i_{th} front of a new population $\mathbf{P}_{t+1}$ for the $(t+1)$ generation according to the geometric distribution is given by the expression

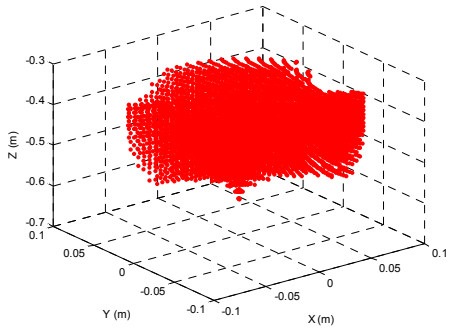

Fig. 3. Workspace volume of 3PRS manipulator.

$$N_i = N\frac{1-r}{1-r^k}r^{i-1}, \tag{35}$$

where r the reduction rate is a user defined parameter and N is the population size, k is the number of non-dominated fronts formed in the current population.

Thus the main concept of CENSGA is to forcibly allow at least a certain number of solutions from each non-dominated front of R_t to co-exist in the new population $\mathbf{P}_{t+1}$ of size N. The new population $\mathbf{P}_{t+1}$ is now used for selection, crossover and mutation to create a population $\mathbf{Q}_{t+1}$ of size N, and then $\mathbf{R}_{t+1}$ is formed by combining $\mathbf{P}_{t+1}$ and $\mathbf{Q}_{t+1}$ for the non-dominated sorting. The selection of a specified number of solutions from each front is achieved by crowded tournament selection.

9. Results and discussion

9.1 Workspace simulation

Symmetric architectures are commonly considered in the literature, so here we also considered a symmetrical 3PRS manipulator having both fixed and moving platforms are equilateral triangles with $a = 0.4$ m, $b = 0.2$ m and leg length l is 0.55 m as an example. The motion ranges of linear actuators are within ± 0.15 m, and the cone angle of the spherical joints is bounded between $0^0 - 50^0$. It is necessary to analyze the shape and size of the workspace volume for enhanced applications of parallel manipulators. The researchable workspace volume of 3PRS manipulator is shown in Fig. 3, which is computed using the inverse kinematic equations through Matlab programming. The workspace volume is continuous and there are no vertical gaps along the Z coordinate; the workspace volume appears like a cylinder in the middle portions and which appears like a triangular pyramid for the top and bottom portions. The cross sectional workspace at the bottom section p_z = -0.37 m is shown in Fig. 4, and appears as an equilateral triangle in shape.

9.2 Dexterity measures of 3PRS PKM

The Condition index (CI) of the manipulator is dependent on the end-effecter's pose; it varies from one point to another

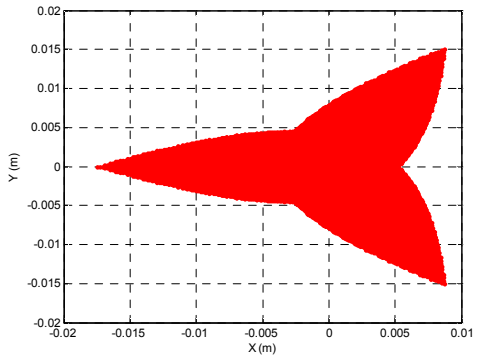

Fig. 4. Workspace of section at $p_z = -0.37$ m.

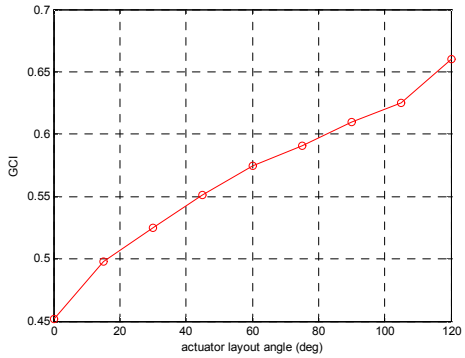

Fig. 5. GCI versus actuator layout angle (α).

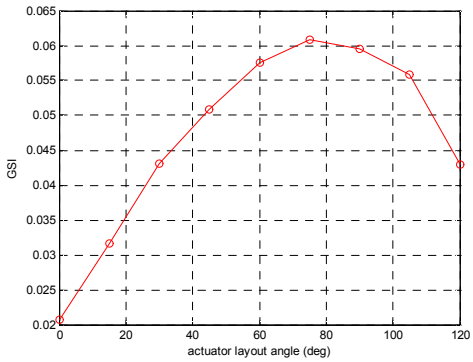

Fig. 6. GSI versus actuator layout angle (α).

point within the workspace, so it is a local measure of performance. To measure the global performance we considered two global performance indices, GCI and GSI. The variation of GCI, GSI with actuator layout angle is shown in Figs. 5 and 6, respectively. It is observed that GCI is continuously increasing with increase of actuator layout angle and reaches its maximum at $\alpha = 120^0$ because at lower actuator layout angles the presence of inverse and direct kinematic singularity regions is more, so the manipulator is uncontrollable and the Jacobian matrix is ill conditioned. Whereas, GSI has its maximum at $\alpha = 78^0$; afterwards a decreasing trend is observed. The reason for this is that at larger actuator layout angles constraint forces due to the architecture singularities can be significant for the given dimension of the 3PRS parallel mechanism. The stiffness ellipsoid is not closer to a hyper sphere; the stiffness is more in one axis and low in other axis. The simulation result of workspace volume with variation of actuator layout angle is shown in Fig. 7. It can be observed that the workspace volume has attained its maximum at $\alpha = 60^0$; after that a continuously decreasing trend is observed. It is necessary to choose an appropriate actuator layout angle so as to achieve an equal compromise between GCI, GSI and workspace volume for enhanced applications of 3PRS manipulator.

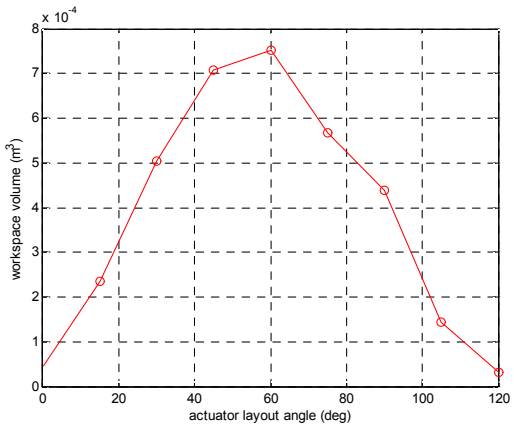

Fig. 7. Effect of actuator layout angle (α) on workspace volume.

9.3 Simulation of GA

Seven GA simulations were performed using the MATLAB optimization toolbox. The first three simulations were performed as a single objective optimization problem to maximize the GCI, GSI and workspace volume separately. As a part of multi-objective optimization, firstly GCI and workspace volume are considered as objectives; secondly, GSI and workspace volume are optimized and then GCI and GSI for the next simulation run. A three objective optimization problem is solved while considering the GCI, GSI and workspace volumes are simultaneously in the final simulation run.

9.3.1 Single-objective GA

The optimal design vector $x = [a \quad b \quad l \quad \alpha]$ for the maximum GCI is to be found as a single objective optimization problem in which the design parameters are allowed to change in the range for $a \in [0.34, 0.44]$, $b \in [0.18, 0.27]$, $l \in [0.4, 0.57]$, $\alpha \in [20^0, 100^0]$, $d_{i\min} \le d_i \le d_{i\max} = \pm 0.15$ m and the cone angle of the spherical joints are bounded between $0^0 - 50^0$. Some preliminary runs to set the GA parameters for simulation of single objective GA are given in Table 1. The GCI is evaluated and the results are shown in Fig. 8; the maximum GCI of 0.6793 is attained for the design vector $x = [0.340 \quad 0.269 \quad 0.537 \quad 93.54^0]$. The GSI is maximized as a second single objective problem which is subjected to the same bound constraints mentioned above. The evolution of GSI as a function of generations is shown in Fig. 9; the maxi-

Table 1. Simple GA parameters.

Parameter	Setting
Population size	60
Maximum generations	100
Encoding type	Real
Selection strategy	Stochastic sampling
Crossover type	Scattered
Mutation type	Adaptive

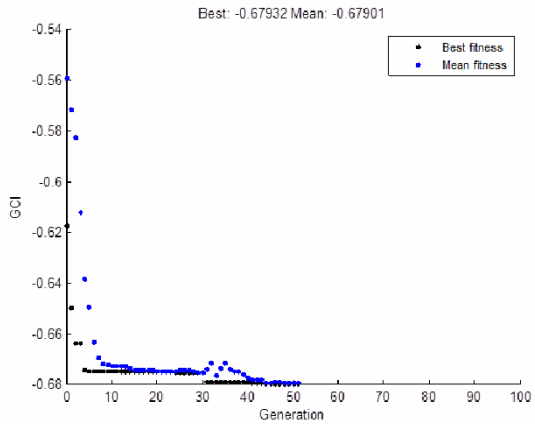

Fig. 8. Convergence of GCI.

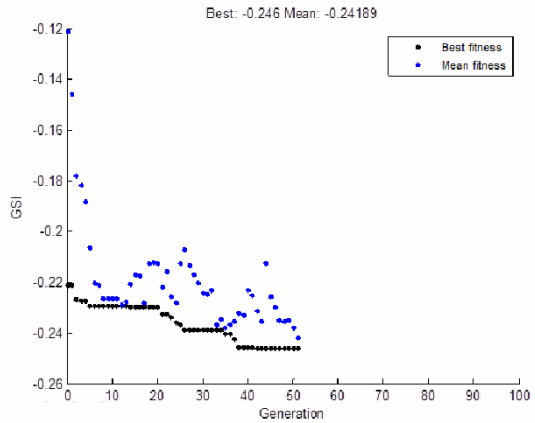

Fig. 9. Convergence of GSI.

mum GSI of 0.246 corresponding to the optimal design vector $x = [0.341 \quad 0.270 \quad 0.521 \quad 83.78^0]$ is attained. In the third GA simulation, the workspace volume is maximized for the same set of bound constraints given above, and the evolution of workspace volume as a function of generations is shown in Fig. 10. The maximum workspace volume of 9.258e-004 m^3 for the design vector $x = [0.421 \quad 0.195 \quad 0.511 \quad 63.79^0]$ is obtained. The design vector is not the same in all the single objective simulation runs for the evolution of maximum fitness values, so it is observed that there is a conflict among the objectives for their optimal values.

The design vector corresponding to the maximum workspace volume of 9.258e-004 m^3 yields the kinematic indices

Table 2. CENSGA algorithm parameters.

Parameter	Setting
Population size	100
Maximum generations	100
Encoding type	Real
Selection strategy	Tournament
Tournament size	2
Crossover type	Intermediate
Crossover ratio	0.6
Mutation type	Adaptive
Reduction factor r	0.7

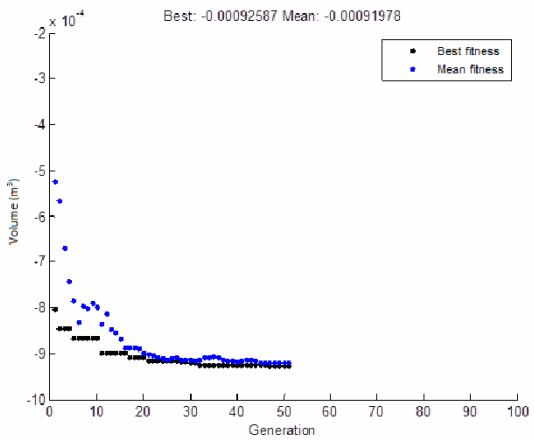

Fig. 10. Convergence of workspace volume.

GCI = 0.5084 and GSI = 0.0437, on comparison of these indices with their optimal (maximized) values of GCI = 0.6793 and GSI = 0.2461, which are much lower. The design vector corresponding to the maximum GSI = 0.246 yields the GCI = 0.663 and workspace volume 1.468e-004; in this case the workspace volume is very small. And also the design vector corresponding to maximum GCI = 0.6793 yields the GSI = 0.239 and workspace volume of 1.066e-004; on comparison of these values with their maximums the GSI is moderately small and workspace volume is much smaller. A larger workspace volume for larger fixed platform and smaller moving platform sizes are observed. For the maximum workspace volume the increase in fixed platform size and decrease in moving platform sizes are 28% and 37%, respectively, when compared with the design vectors corresponding to the maximum dexterity indices.

9.3.2 Simulation of multi-objective optimization

This section develops several experiments while optimizing the three objective functions GCI, GSI and workspace volume. After some preliminary simulations, the set simulation parameters to run the CENSGA are given in Table 2. First, a two objective optimization by considering two objectives simultaneously (GCI vs. volume, GSI vs. volume, GCI vs. GSI) is performed and the corresponding final approximation sets are

Table 3. Pareto optimal solutions three objective optimization.

$x=[a \quad b \quad l \quad \alpha]$				GCI	GSI	Volume (m^3)
0.3434	0.2695	0.5336	80.755^0	0.6720	0.2439	0.0001
0.3735	0.2453	0.5302	73.015^0	0.6330	0.1564	0.0004
0.4350	0.1935	0.5571	58.364^0	0.5173	0.0440	0.0010
0.3544	0.2670	0.5321	80.692^0	0.6615	0.2303	0.0002
0.4124	0.2251	0.5261	68.258^0	0.5728	0.0980	0.0007
0.4328	0.2354	0.5149	57.177^0	0.5514	0.1098	0.0008
0.3820	0.2375	0.5297	73.229^0	0.6061	0.1294	0.0005
0.4301	0.2585	0.5190	64.077^0	0.5925	0.1796	0.0007
0.4326	0.2248	0.5222	58.120^0	0.5387	0.0880	0.0009
0.4330	0.2561	0.5278	68.667^0	0.5969	0.1758	0.0006

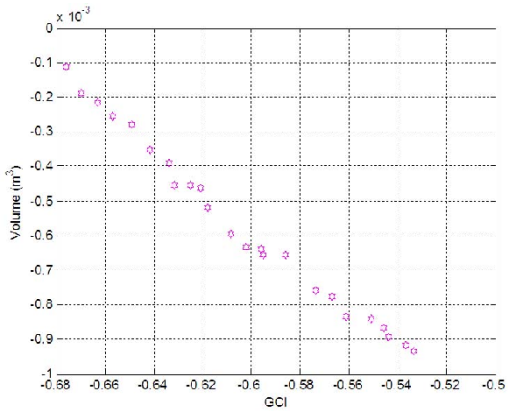

Fig. 11. Pareto front for GCI and volume.

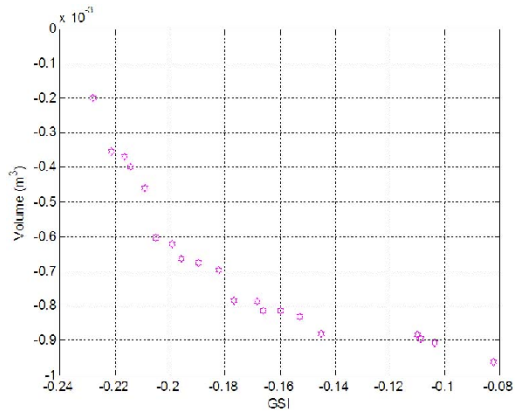

Fig. 12. Pareto front for GSI and volume.

shown in Figs. 11-13, respectively. The final approximation front for GCI vs. volume is achieved by varying the design parameters in a specific range, which is observed for $a=[0.355\ 0.431], b=[0.227\ 0.268], l=[0.498\ 0.532]$ and for $\alpha=[56.34^0\ 89.93^0]$. The design parameters for final approximation front for GSI vs. volume varies for $a=[0.383\ 0.434]$, $b=[0.222\ 0.266]$, $l=[0.509\ 0.521], \alpha=[56.80^0\ 79.54^0]$. The design parameters for final approximation front between GCI

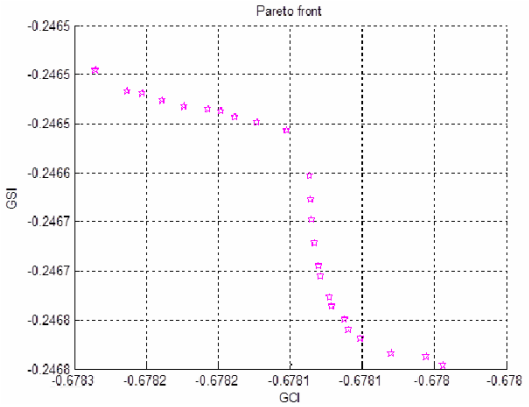

Fig. 13. Pareto front for GCI and GSI.

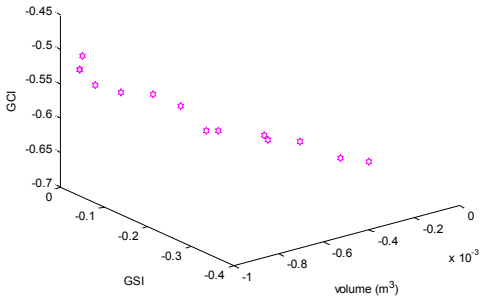

Fig. 14. Pareto front for GCI, GSI and volume.

and GSI are varied as for $a=[0.341\ \ 0.342], b=[0.2700\ 0.2701], l=[0.4808\ 0.4809]$ and for $\alpha=[88.66^0\ \ 89.01^0]$.

In the second simulation of multi-objective optimization the three objective functions GCI, GSI and workspace volume are optimized simultaneously for the same CENSGA parameters that are set for a two objective optimization. The three-dimensional final approximation set in criterion space is shown in Fig. 14 and the some non-dominated solutions of the final approximation set corresponding to the three objectives are given in Table 3. The final approximation front is achieved by varying the design parameters in a specific range, which is $a=[0.343\ \ 0.435], b=[0.193\ \ 0.267], l=[0.514\ \ 0.557]$ and for $\alpha=[57.17^0\ \ 80.75^0]$. The design parameter α is greatly influencing the GSI in which higher GSI index for the solutions having larger actuator layout angles; when the actuator layout angle is approaching 90^0 the three rails A_iN for $i=1,2,3$ become vertical and the compliance is minimum. While in a three objective optimization the functional variation of GCI and workspace volume in a dimensional approximation set is shown in Fig. 15, in which it is observed that GCI and workspace volume are quarrelsome with each other for their optimal values. The ideal solution would be maximizing both the functions so as an intermediate solution is to be chosen depending on the designer's choice. The final approximation set for GSI and workspace volume in a three objective optimization is shown in Fig. 16, in which it is observed that they are quarrelsome with each other and form a convex Pareto front. The final approximation set for GCI and GSI is also shown in

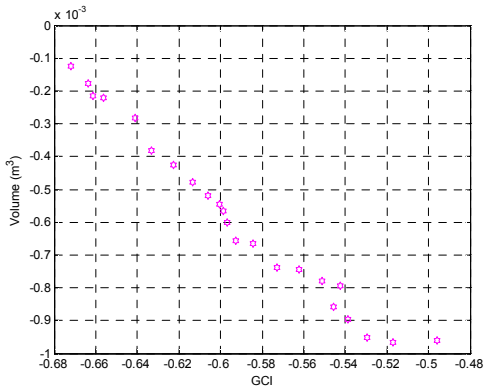

Fig. 15. Pareto front for GCI and volume.

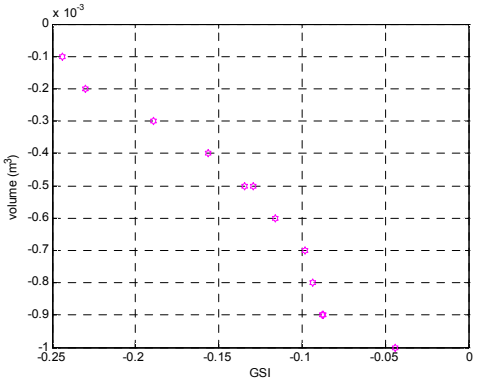

Fig. 16. Pareto front for GSI and volume.

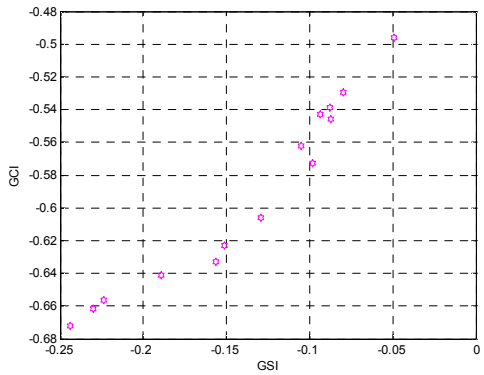

Fig. 17. Pareto front for GSI and GCI.

Fig. 17; the objectives are linearly quarrelsome with each other in which GCI and GSI can follow a similar approach such as one is increasing and the other one is also increasing.

10. Conclusions

A complete kinetostatic design methodology for the development of general 3PRS parallel manipulator has been provided. The global stiffness matrix of a general 3PRS parallel mechanism was derived by considering the actuator compliance, leg axial and bending compliances by compliant modeling. The workspace performance indices GCI, GSI and workspace volumes were quantified at various actuator layout angles; the workspace volume, GSI, GCI are maximum at 60^0, 78^0, 120^0 of the actuator layout angles, respectively; these results are helpful in designing suitable actuator layout angle. The architecture optimization for a general 3PRS parallel manipulator is carried out by solving a multi-objective optimization problem in order to obtain a larger reachable workspace with improved global condition index and global stiffness indexes. The architectural optimizations developed are successfully implemented in MATLAB environment for a single objective optimization as well as for multi-objective optimizations. The adopted algorithm CENSGA is a robust optimization tool that provides a final approximation set with widely spread non-dominated solutions. The design vector corresponding to maximum workspace volume registers only 17% and 70% of their maximum GSI, maximum GCI, respectively. The design vector corresponding to the maximum GSI registers only the 18% and 80% of their maximum workspace volume and maximum GCI, respectively; it relies on the necessity of multi-objective optimization. The simulation results provide a sound basis for optimization of manipulators that are appropriate for different specific applications. Although the procedure developed is for 3PRS parallel manipulator, this approach can be extended to other types of parallel manipulators.

Acknowledgment

The authors are grateful to the anonymous reviewers for their critical and constructive review of the manuscript.

References

[1] D. Stewart, A platform with six degrees of freedom, *Proc. of the Institute of Mechanical Engineers,* 180 (1) (1965) 371-386.

[2] The DS Technology Company, *http:// www.ds-technologie*. De (2008).

[3] N. Hennes, Ecospeed: an innovative machining concept for high performance 5-axis machining of large structural component in aircraft engineering, *Proc.of the 3rd Chemnitz Parallel Kinematic Seminar,* Chemnitz, Germany (2002) 763-774.

[4] J. A. Carretero, M. Nahon, C. M. Gosselin and B. Buckham, Kinematic analysis of a three-dof parallel mechanism for telescope applications, *Proc.of the ASME Design Automation Conference,* Sacramento, California, USA (1997).

[5] X. Han, Y. Wang and J. Shi, Stiffness modeling of 3PRS mechanism, *World Academy of Science, Engineering and Technology*, 72 (2012) 876-882.

[6] M. S. Tsai, T. N. Shiau and Y. J. Tsai, Direct kinematic analysis of a 3-PRS parallel mechanism, *Mechanism and Machine Theory*, 38 (1) (2003) 71-83.

[7] F. Zhang, J. G. Yang and B. Z. Li, Kinematic characteristic analysis of 3-PRS parallel manipulator, *Donghua U.*, 25

(2008) 78-81.
[8] Y. Li and Q. Xu, Kinematic analysis of a 3-PRS parallel manipulator, *Robotics and Computer-Integrated Manufacturing*, 23 (2007) 395-408.
[9] X. Chen, X. Liu, F. Xie and T. Sun, A comparison study on motion/force transmissibility of two typical 3-DOF parallel manipulators: The Sprint Z3and A3 tool heads, *International J. of Advanced Robotic Systems*, 11 (5) (2013) 1-10.
[10] C. Gosselin and J. Angeles, A global performance index for the kinematic optimization of Robotic manipulators, *J. of Mechanical Design*, 113 (3) (1991) 220-226.
[11] A. Fattah and A. M. H.Ghasemi, Isotropic design of spatial parallel manipulators, *International J. of Robotics Research*, 21 (9) (2002) 811-824.
[12] J. P. Merlet, Workspace-oriented methodology for designing a parallel manipulator, *Proc.of IEEE International Conference on Robotics and Automation*, Minneapolis, Minnesota, USA (1996) 3726-3731.
[13] J. Wang, C. Wu and X. Liu, Performance evaluation of parallel manipulators: motion/force transmissibility and its index, *Mechanism and Machine Theory*, 45 (10) (2010) 1462-1476.
[14] Z. Gao, D. Zhang, X. Hu and Y. Ge, Design, analysis and stiffness optimization of a three degree of freedom parallel manipulator, *Robotica*, 28 (3) (2010) 349-357.
[15] X. Liu, Z. Jin and F. Gao, Optimum design of 3-DOF spherical parallel manipulators with respect to the conditioning and stiffness indices, *Mechanism and Machine Theory*, 35 (9) (2000) 1257-1267.
[16] S. Lu and Y. Li, Dimensional synthesis of a 3-DOF translational parallel manipulator considering kinematic dexterity property, *Proc.of the IEEE International Conference on Information and Automation*, Hailar, China (2014) 7-12.
[17] F. A. Lara-Molina, J. M. Rosario and D. Dumur, Multi-objective design of parallel manipulator using global indices, *The Open Mechanical Engineering J.*, 4 (2010) 37-47.
[18] R. Kelaiaia, O. Company and A. Zaatric, Multi-objective optimization of a linear Delta parallel robot, *Mechanism and Machine Theory*, 50 (2012) 159-178.
[19] G. Wu, Stiffness analysis and optimization of a co-axial spherical parallel manipulator, *Modeling, Identification and Control*, 35 (1) (2014) 21-30.
[20] S. S. Ganesh, A. B. K. Rao and S. Darwekar, Multi-objective optimization of 3-DOF translational parallel kinematic machine, *J. of Mechanical Science and Technology*, 27 (12) (2013) 3797-3804.
[21] C. Guohua, W. Bin, W. Nan and Z. Yanwei, Stiffness, workspace analysis and optimization for 3UPU parallel robot mechanism, *Telkomnika,* 11 (9) (2013) 5253-5261.
[22] J. A.Carretero, M. A. Nahon and R. P. Pondhorodeski, Workspace analysis and optimization of a novel 3-DOF parallel manipulator, *International J. of Robotics and Automation*, 15 (2000) 178-188.
[23] Y. Li and Q. Xu, Optimal kinematic design for a general 3PRS spatial parallel manipulator based on dexterity and workspace, *Proc.of the Eleventh International Conference on Machine Design and Production*, Antalya, Turkey (2004).
[24] X.-J. Liu and I. A. Bonev, Orientation capability, error analysis and dimensional optimization of two articulated tool heads with parallel kinematics, *J. of Manufacturing Science and Engineering*, 130 (2008) 1-9.
[25] G. Pond and J. A.Carretero, Architecture optimization of three 3-PRS variants for parallel kinematic machining, *Robotics and Computer-Integrated Manufacturing,* 25 (1) (2009) 64-72.
[26] X. Zhang, Optimization of a 3-PRS parallel manipulator based on interval analysis, *Proc.of Intelligent Control and Automation*, Beijing, China (2012) 2452-2456.
[27] G. Carbone and M. Ceccarelli, Comparison of indices for stiffness performance evaluation, *Frontiers of Mechanical Engineering China*, 5 (1) (2010) 270-278.
[28] K. Deb and T. Goel, Controlled elitist non-dominated sorting genetic algorithms for better convergence, E.Zitzler et al. (Eds), *EMO 2001,LNCS 1993* (2001) 67-81.
[29] E. Zitzler, Evolutionary algorithms for multi-objective optimization: methods and application, *Doctoral Dissertation ETH 13398*, Swiss Federal Institute of Technology, Zurich, Switzerland (1999).
[30] J. Knowles and D. Corne, The Pareto archived evolution strategy: A new base line algorithm for multi-objective optimization, *Proc.of the 1999 Congress on Evolutionary Computation,* Piscat asway, NJ: IEEE Press (1999) 98-105.
[31] K. Deb, A. Pratap, S. Agarwal and T. Meyarivan, A fast and elitist multi-objective genetic algorithm: NSGA-II, *IEEE Transactions on Evolutionary Computation,* 6 (2) (2002) 182-197.

S. Ramana Babu received the M.Tech. in 2006 from the Jawaharlal Nehru Technology University. Currently, he is an Assistant Professor in Raghu Engineering College, Visakhapatnam, India. His research interests include design and simulation of parallel manipulators.